Dendrimer−Polyelectrolyte Complexation: A Model Guest−Host System

P. Welch and M. Muthukumar*

Polymer Science and Engineering Department, University of Massachusetts, Amherst, Massachusetts 01003

Received January 6, 2000; Revised Manuscript Received April 24, 2000

ABSTRACT: Much experimental effort to realize possible uses of dendrimers has focused on the complexation of charged dendrimers to oppositely charged polyelectrolytes to form controlled delivery systems. Employing computer simulation and theory, we present a molecular-level picture of these guest−host aggregates and the conditions necessary for forming them. Specifically, we examine the equilibrium and dynamic complexation behavior of a monocentric dendrimer with charged terminal groups to a flexible, oppositely charged polyelectrolyte. Three different types of complexes are noted depending upon the solution ionic strength and the sizes of the dendrimer and chain. We find that a dendrimer may encapsulate a chain, a chain and a dendrimer may mutually interpenetrate, or a unique "chain-walking" phenomenon may be observed. The critical conditions for complexation, density profiles of the polyelectrolyte and the dendrimer in the complex, and the curious dynamics observed are discussed. A closed formula is proposed to describe the critical conditions for complexation between a dendrimer and a polyelectrolyte.

1. Introduction

There has recently been an increased interest in studying complexation between polyelectrolytes and oppositely charged entities.[1−15] The dendritic polymer topology offers many unique and interesting opportunities within this context. The growing list of possible applications includes their use as molecular cages and controlled delivery agents.[16] Pioneering experimental work has been carried out to explore and develop these proposed uses for dendrimers.[16−24] Much of this effort has focused on the complexation of charged dendrimers to oppositely charged polyelectrolytes. Of particular note are the DNA transport studies of Kukowska-Latallo and Ottaviani and their co-workers,[20−22] the light scattering investigation of polycation−dendrimer complexation by Li et al.,[23] and the potentiometric titration studies of Kabanov et al.[24] These works clearly demonstrate that charged dendrimers may be employed to capture and transport oppositely charged polyelectrolytes. Although these experimental works elegantly demonstrate the potential these molecules possess to fulfill this role, a clear understanding of the criteria to form these complexes and the attendant molecular behavior is not easily discerned. Here, we attempt to elucidate a clearer molecular-level picture via analytical and computer simulation techniques. Specifically, we examine the equilibrium complexation behavior of a monocentric dendrimer with charged terminal groups to a flexible, oppositely charged polyelectrolyte in solutions. Our approach is to investigate the molecular nature of the complex via bond-fluctuation Monte Carlo simulations and to predict the critical complexation conditions with a variational calculation. Questions pertaining to the chain location within the complex, the permeability of the dendrimer, and the change in dimension of both species upon complexation are addressed.

In section 2 we present the computer simulation model and technique used to calculate the equilibrium behavior of the complexes. The results of our simulations are presented in section 3. In section 4 we present our analytical prediction for the critical complexation conditions and a comparison of that result with our simulations. The significance of our findings are discussed in light of the above-mentioned experimental work in section 5, and we make some concluding remarks in section 6.

2. Simulation Model and Algorithm

2.1. Model. A bead−spring, united atom model was employed to represent both the monocentric dendrimer with charged terminal groups and the fully charged chain electrolyte. The springs serve to maintain the topological connectivity in the molecules and have the same average length in both. The beads represent the mass and are the sites of the pairwise interactions. All beads are of the same diameter, d. Three generations of dendritic growth, 4, 5, and 6, and three chain molecular weights, 15, 30, and 60, were examined. The terminal groups of the dendrimer and every bead on the chain have charge qe, where e is the fundamental unit of charge. The charge−charge interaction between the two molecules is attractive, corresponding to the interaction of a polyanion with a polycation. Charged beads are illustrated in black and gray in Figure 1. This model is analogous to the experimentally realizable system of an ammonia core based dendritic poly(amidoamine)[25] or dendritic poly(propyleneimine)[26] with charged terminal groups complexing to a flexible polyelectrolyte such as poly(acrylic acid).

2.2. Energetics. This simulation incorporated three classes of interactions: bonded, excluded volume, and Coulombic. The "finitely extensible nonlinear elastic" (FENE)[27] potential was employed to maintain the bond constraints and is given by eq 1.

$$\frac{U_B}{k_B T} = -KR^2\left(\sum_{i=1}^{N_L-1}\log\left[1-\left(\frac{l_i-l_o}{R}\right)^2\right]+\sum_{i=1}^{N_D-1}\log\left[1-\left(\frac{l_i-l_o}{R}\right)^2\right]\right) \quad (1)$$

Here, N_D and N_L are the number of dendritic and linear beads, respectively. K is the spring constant and is set to $20.0/l_B^2$. $R = l_{max} - l_o$ where $l_o = (l_{max} + l_{min})/2$. l_i,

10.1021/ma000021d CCC: $19.00
Published on Web 07/19/2000

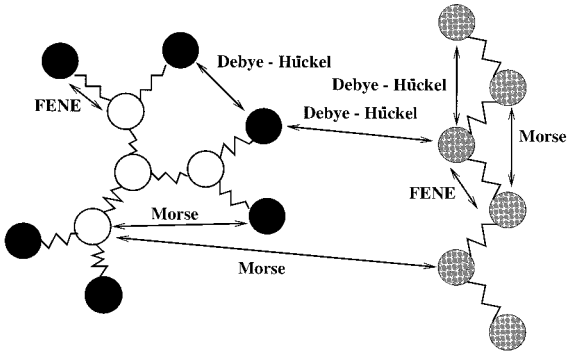

Figure 1. Bead−spring model used in simulations. The chain and dendrimer have oppositely charged beads, shaded in gray and black.

l_{max}, and l_{min} are the bond length of bond i, the maximum, and the minimum bond lengths, respectively. The values of these parameters were chosen to scale the simulation lengths by the Bjerrum Length, l_B (defined below), and to prevent the occurrence of "phantom chains". The value of l_B in water at 25 °C is 7.1 Å. In synthetic dendrimers, the distance between branch points is estimated to be on the order of 5 Å. Thus, we have taken $l_o = 0.7l_B$, $l_{max} = 1.0l_B$, and $l_{min} = 0.4l_B$ for both the dendrimer and the linear chain. Rather than calculate the FENE potential exactly for every new state generated in the simulation, a table of discrete energy values was created at the beginning of the simulations. The bonded interactions were thus approximated by searching the table for the energy value that most closely corresponded to the calculated bond length. A Δl_i value of $6.00 \times 10^{-4} l_B$ was used in creating the table.

The electrostatic attractions and repulsions were approximated by the Debye−Hückel potential,[28] eq 2.

$$\frac{U_C}{k_B T} = l_B|q|^2 \sum_{i,j=1}^{N_T'} \frac{e^{-\kappa r_{ij}}}{r_{ij}} + l_B|q|^2 \sum_{i,j=1}^{N_L} \frac{e^{-\kappa r_{ij}}}{r_{ij}} - l_B|q|^2 \sum_{i=1}^{N_T'} \sum_{j=1}^{N_L} \frac{e^{-\kappa r_{ij}}}{r_{ij}} \quad (2)$$

The primes indicate summation over only the terminal groups of the dendrimer. N_T is the number of dendritic terminal groups, and r_{ij} is the distance between two charged beads. The inverse Debye length, κ, is a measure of the solution ionic strength and is given by

$$\kappa^2 = 4\pi l_B \sum_i c_i z_i^2 \quad (3)$$

$$l_B = \frac{e^2}{4\pi\epsilon_0 \epsilon k_B T} \quad (4)$$

Here, c_i and z_i are the concentration and valence of the ith ion, respectively. ϵ_0 is the permittivity of vacuum, and ϵ is the dielectric constant. κ^{-1} was varied from $0.42l_B$ to $42.0l_B$, spanning the range of aqueous salt concentrations from 1 M to 0.1 mM at 25 °C. In the limit of high solvent ionic strength the potential falls off rapidly but is long ranged in the low salt concentration limit. We have studied different values of $|q| = 1.0$, 0.5, and 0.1. In realistic situations, smaller counterions may play a substantial role, and at present the correct form of the potential between two charges on two macromolecules in an electrolyte solution is not known. To facilitate an understanding of the large-scale behavior of complexation between macromolecules, we have assumed the Debye−Hückel potential between two charges, without explicitly deriving this.

Finally, the excluded-volume interactions between all the beads in the system were modeled by eq 5, the Morse[28] potential.

$$\frac{U_E}{k_B T} = \frac{\sigma'}{k_B T} \sum_{i=1}^{N_L} \sum_{j=1}^{N_D} [(e^{-\alpha'(r_{ij}-d)} - 1)^2 - 1] + \frac{\sigma}{k_B T} \sum_{i,j=1}^{N_L} [(e^{-\alpha(r_{ij}-d)} - 1)^2 - 1] + \frac{\sigma}{k_B T} \sum_{i,j=1}^{N_D} [(e^{-\alpha(r_{ij}-d)} - 1)^2 - 1] \quad (5)$$

σ and α^{-1} are respectively the strength and range parameters employed for the intramolecular potentials. In this study, $\alpha^{-1} = l_B/24$ and $d = 0.8l_B$ in order to prevent bond crossing and to provide a short truncation length of $3.5l_B$ for the interaction.[29] σ was chosen as our fundamental unit of energy and solvent quality was determined by $k_B T$. The simulation was carried out in a "good" solvent regime for both molecules with $k_B T = 0.7\sigma$.[29,30] Different values for the strength and range parameters were used for the intermolecular interactions. To mimic a purely hard-bead interaction, α'^{-1} and σ' were assigned the values of $l_B/80.0$ and 0.01σ, respectively. As in the case of the FENE potential, a discrete table of energy values was generated at the beginning of the simulations and used to approximate the Morse energy values. A value of Δr_{ij} equal to $8.75 \times 10^{-4} l_B$ was used in constructing this table.

2.3. Algorithm. A generalization to multiple molecules of the algorithm presented in ref 31 was employed in this study. Bond fluctuation was accomplished by randomly displacing beads by ΔX, ΔY, and ΔZ in the range $\pm 0.5 l_B$ and constraining the bond lengths to lie within the above-stated bounds. The transition to each new state, corresponding to a new link in the Markovian chain, was accepted with the Metropolis criteria.[32] Specifically, a new conformation was generated and the change in energy, $\Delta U = \Delta U_B + \Delta U_C + \Delta U_E$, computed. If the system decreased in energy, the new state was accepted. Otherwise, a random number between 0 and 1 was obtained, and the new state was accepted if the random number was less than the Boltzmann factor for the transition, $e^{-\Delta U/k_B T}$.

The simulations were carried out in two stages. First, the chain and dendrimer were equilibrated in isolation at a given ionic strength. A linear rod was used as an initial configuration for the chains. Depending upon molecular weight, statistics for the chains were accumulated over 5−10 million Monte Carlo steps (MCS), each step comprising a number of attempted perturbations equal to the chain length. Samples from the ensemble were taken at a frequency of 1 every 10 000−40 000 MCS, varying with chain length. Similarly, an initially random, self-avoiding dendrimer was simulated for 5−10 million MCS, and statistics were gathered once every 10 000 MCS. The sample frequencies were determined using standard statistical techniques[33] and were chosen to ensure that statistically independent values were averaged. In both cases, the ensemble average radius of gyration for each molecule was calculated to monitor the approach to equilibrium.

Next, samples from the equilibrium ensembles generated in the single molecule simulations were placed in close proximity to one another, usually $7l_B-3l_B$ apart. The bond-fluctuation algorithm then continued for 5 million more MCS, and the population was sampled every 10 000 MCS after an initial 1 million MCS had elapsed for complexation and equilibration. Slow relaxation processes may be expected to be operational in this system. However, to verify that complexation did or did not occur for values of κ near the critical value, samples from complexes equilibrated under lower ionic strengths were used as initial conditions. The critical value of κ demonstrated no dependence on the initial condition used, and the ensemble averages obtained proved independent of both initial conditions and Monte Carlo trajectory (differing random number seed). Thus, though the statistics may not be rigorously uncorrelated, we do expect that they are representative of equilibrium complexes.

The instantaneous adsorption energy defined as the total interaction between the dendrimer and the chain, $E_a = U_E + U_C$, was calculated to monitor the approach to equilibrium. Ensemble averages of several conformational characteristics were obtained postsimulation. The mean-square radii of gyration for the chain, $\langle R_g^2\rangle_L$, and the dendrimer, $\langle R_g^2\rangle_D$, in the complex were calculated. Further, to facilitate a clear picture of the chain's location relative to the dendrimer, the dendrimer-centered chain density profile, $\langle\rho\rangle_L$, and dendrimer terminal group density profile, $\langle\rho\rangle_T$, were calculated postsimulation using eq 6.

$$\langle\rho(r)\rangle = \langle n(r)\rangle\frac{V_b}{V_s(r)} \tag{6}$$

$\langle n(r)\rangle$ is the ensemble average number of beads in the shell at distance r. V_b and $V_s(r)$ are the volumes of the beads and shells, respectively.

3. Simulation Results

3.1. Dendrimer Density Profile. As described below, the role of the chain in the guest−host system depends on several variables. However, the basic requirement for the encapsulation of a molecule by the dendrimer is the presence of dendritic cavities. Previously, we proposed the conditions under which flexible dicentric dendrimers with charges at each branch and terminal group might form such cavities.[31] In this study, we also find that the density profile of monocentric dendrimers with charges at only the terminal groups may be similarly tuned with ionic strength of the solution. For generations 4 and 5, $\langle\rho\rangle_D$ is found to be monotonically decreasing[34] in the high salt limit, and a pronounced depression[35] is observed near the center of the dendrimer in the low salt limit for generation 5. Generation 6 presents similar behavior in the low salt limit but also expresses a dip in density one bead diameter away from the center in the high salt limit due to the strong correlation of the location of the first three branch points as noted in other theoretical studies.[36,37] This behavior is illustrated in Figure 2.

The radial distribution of charged terminal groups is critical in determining the complexation conditions, as suggested by our variational result discussed below. For all generations of growth, the location of the terminal groups was found to be distributed throughout the molecule in the high salt limit and pushed to the periphery in the low salt regime. This is illustrated in Figure 3. Note that the depletion of terminal groups near the center for all solvent conditions yields a consistently higher value for $\langle R_g^2\rangle_T$, the squared radius of gyration for the terminal groups, than that for the total molecule. This is illustrated for generation 6 in Figure 4.

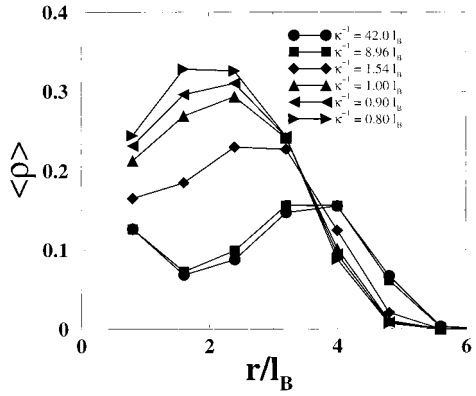

Figure 2. Typical dendrimer density profiles. Data for sixth generation with $|q| = 1.0$ shown.

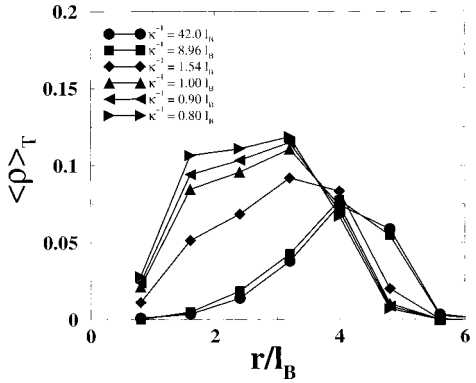

Figure 3. Typical dendrimer terminal group distributions. Data for sixth generation with $|q| = 1.0$ shown.

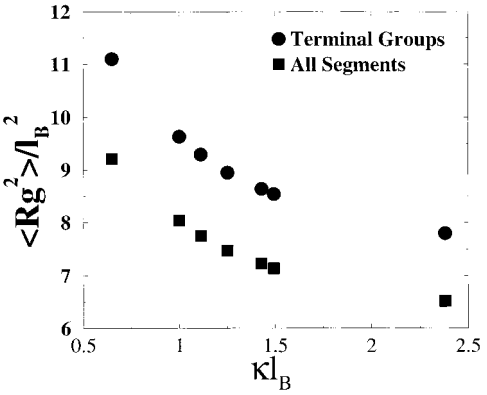

Figure 4. Typical dendrimer $\langle R_g^2\rangle$ and $\langle R_g^2\rangle_T$ behavior as a function of κ. Data for sixth generation with $|q| = 1.0$ shown.

3.2. Complexation-Induced Collapse. In all cases both the dendrimer and the chain shrank in their radial dimension upon complexation. This change in size is illustrated in Figures 5−7. Figure 5 presents $\langle R_g^2\rangle_L^{1/2}$ for a 30-bead chain. Note that as κ increases, the size of the complexed chain approaches that of the chain in free solution. Similar behavior was observed for 15 bead chains. Sixty bead chains present a more complicated picture, as illustrated in Figure 6. For complexes formed with generation 5 and 6 dendrimer, the above-noted

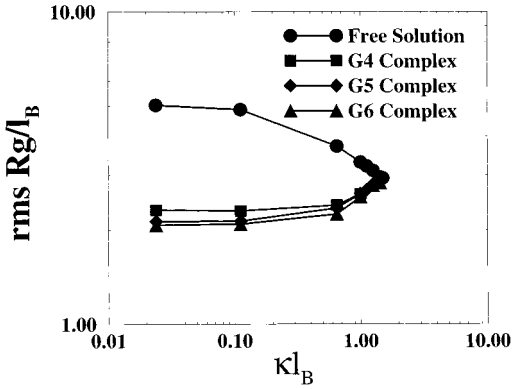

Figure 5. $\langle R_g^2\rangle_L^{1/2}$ as a function of κ and complexing dendrimer generation. Data for 30-bead chain with $|q| = 1.0$ shown.

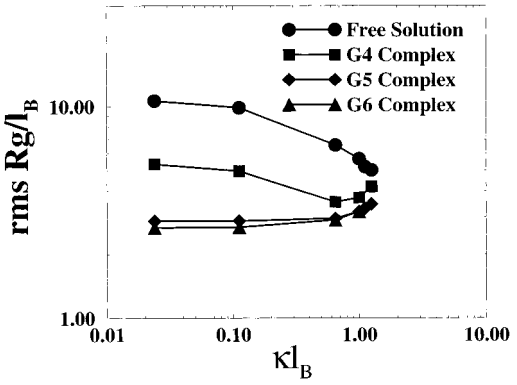

Figure 6. $\langle R_g^2\rangle_L^{1/2}$ as a function of κ and complexing dendrimer generation. Data for 60-bead chain with $|q| = 1.0$ shown.

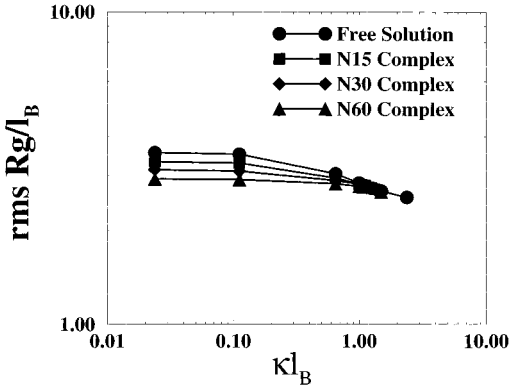

Figure 7. $\langle R_g^2\rangle_D^{1/2}$ as a function of κ and complexing chain length. Data for sixth generation with $|q| = 1.0$ shown.

behavior was recovered. However, generation 4 appears to interact with the 60-bead chain in a markedly different fashion than the larger dendrimers yielding a much smaller change in chain size. Note that the apparent dip in $\langle R_g^2\rangle_L^{1/2}$ for the generation 4 complex at $\kappa l_B \approx 0.6$ is within the standard deviation of $\pm 0.5 l_B$. The dendrimers displayed much more uniform behavior. In all cases the dendrimer shrank upon complexation and approached the free solution limit with increasing ionic shielding, as illustrated in Figure 7.

3.3. Guest−Host Behavior. Three types of complexes were observed to form depending upon the solution ionic strength and relative sizes and charge densities of the molecules. Varying these parameters led to a continuous transition from one type of complex to another. Nevertheless, this qualitative classification

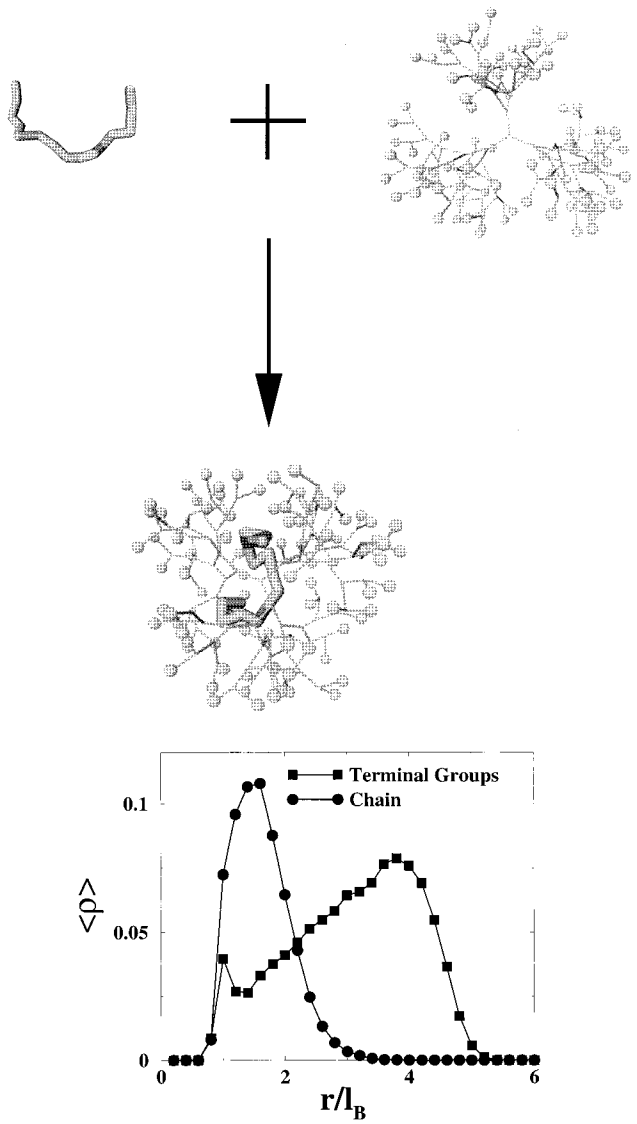

Figure 8. (top) Encapsulation of a 15-bead chain by a sixth generation dendrimer with $\kappa^{-1} = 42.0 l_B$ and $|q| = 1.0$. (bottom) Terminal group and chain density profiles.

scheme presented below is useful for understanding the variety of behaviors that may be realized in these systems. (i) For large dendrimers and short chains, the dendrimer encapsulates the chain and the chain collapses to a coil wrapped within the dendrimer. This is clearly demonstrated when the distribution of terminal groups is compared to the density of chain segments about the center of the dendrimer. Figure 8 illustrates this for a generation 6 dendrimer complexed to a 15-bead chain with $\kappa^{-1} = 42.0 l_B$ and $|q| = 1.0$. For visual contrast, all chains are rendered as worms, and only the terminal groups of the dendrimer are drawn as beads. Here, the chain is seen to fall completely within the radial location of the maximum terminal group density. This behavior is representative of complexes between small chain electrolytes and large dendrimers.

(ii) The second type of complex is one in which the chain not only penetrates but also has significant density outside of the dendrimer. This is illustrated in Figure 9 for a generation 5 dendrimer complexed to a 60-bead chain with $\kappa^{-1} = 1.0 l_B$ and $|q| = 1.0$.

(iii) In the limit of the smallest dendrimer and largest chain studied, closest to a true polymer−dendrimer system, a unique complex is formed in which the

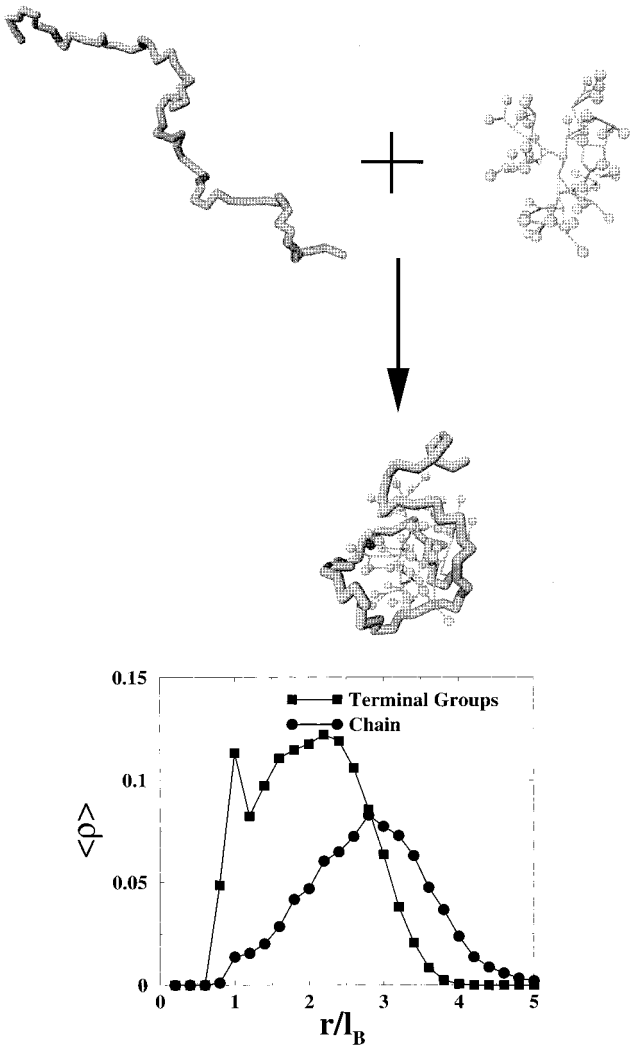

Figure 9. (top) Encapsulation of a fifth generation dendrimer by a 60-bead chain with $\kappa^{-1} = 1.0l_B$ and $|q| = 1.0$. (bottom) Terminal group and chain density profiles.

dendrimer does not possess sufficient charge to shield the chain's self-repulsion to the extent that the chain will shrink. In this case, the chain is only perturbed from its stretched behavior in the immediate vicinity of the dendrimer. This is illustrated by Figure 10 in which a generation 4 dendrimer has complexed to a 60-bead chain at the solution ionic strength, $\kappa^{-1} = 8.96l_B$ and $|q| = 1.0$. Note that near the dendrimer the chain has coiled but that the rest of the chain remains extended. In addition to the "ball-and-chain" configuration shown here, the complex demonstrates interesting and novel dynamics: the dendrimer is observed to "walk" along the chain. Because of the fluctuations in both chain and dendrimer conformations, the dendrimer illustrated in Figure 11 is observed to migrate from one chain end at 3.89×10^6 MCS to the other chain end at 4.89×10^6 MCS. The dendrimer's migration is not deterministic, beginning at one end and moving toward the other before reversing direction, but the dendrimer is observed to complete several laps in the course of the simulation. This type of complex was observed for all values of κ^{-1} above the critical value for 60-bead chains and generation 4 dendrimer. Though similar behavior has been observed for polyelectrolyte−sphere complexes,[14] Monte Carlo does not capture actual dynamics, and this chain-walking phenomenon may prove to be

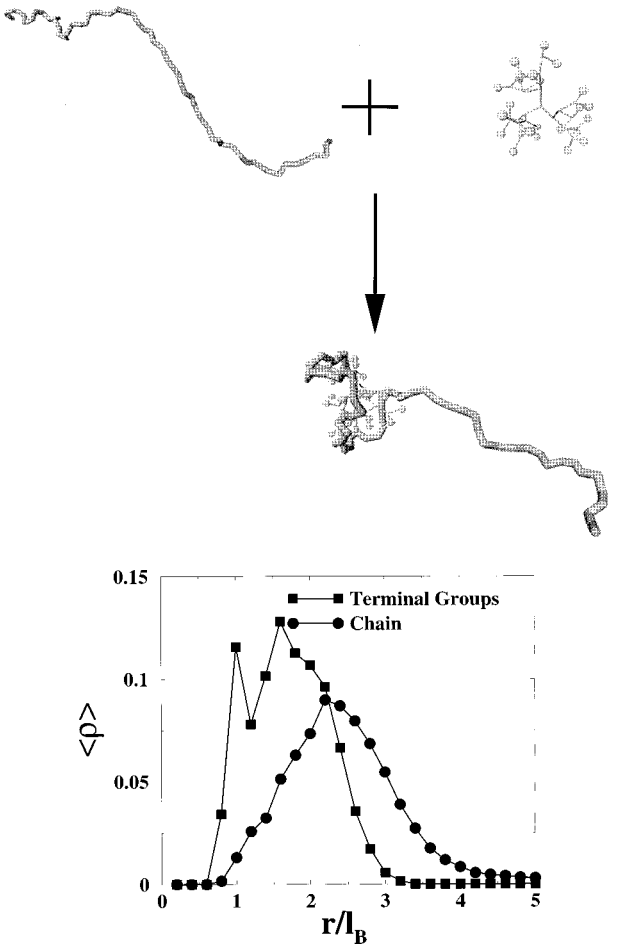

Figure 10. (top) The "ball and chain" configuration of a 60-bead chain complexing to a fourth generation dendrimer with $\kappa^{-1} = 8.96l_B$ and $|q| = 1.0$. (bottom) Terminal group and chain density profiles.

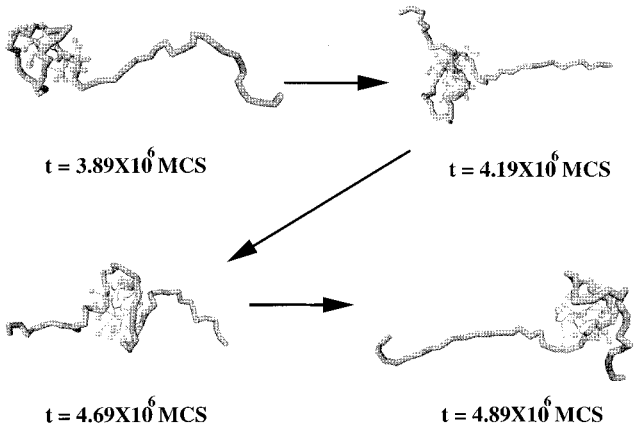

Figure 11. Fourth generation dendrimer "walking" along a 60-bead chain with $\kappa^{-1} = 8.96l_B$ and $|q| = 1.0$.

only a transient. Thus, this dynamic behavior will be further explored in a separate publication.

The above-described complexes are qualitatively different from complexes[13] formed by two oppositely charged polyelectrolytes.

4. Critical Complexation Conditions

4.1. Theoretical Prediction. Complexation was observed to occur for a broad range of solution ionic strengths for all combinations of dendrimer and chain molecular weights studied. However, to identify the

conditions necessary for complexation, we resort to a theoretical technique. Much analytical effort has been applied to the study of adsorption of a polyelectrolyte molecule to various surfaces.[1−12] Particularly germane to the current investigation is our earlier work by von Goeler and Muthukumar,[5] where a polyelectrolyte interacting via the Debye−Hückel potential with a single, impenetrable sphere of opposite charge was considered. Working within the ground-state-dominance approximation and using the variational technique, we derived the critical conditions necessary for complexation to occur in terms of various molecular and solvent parameters. A straightforward extension of this analytical approach yields insight into the question addressed in this paper. Below, we only present our model and result. A brief outline of the derivation is presented in the Appendix. However, we refer the reader to ref 5 for further details of the technique.

The conditions for complexation between the dendrimer and polymer may be expected to be dictated by the nature of the system prior to contact between the two species.[5,15] The dendrimer may therefore be viewed as acting only as an electrostatic potential source and physical barrier. The dendritic charge distribution due to the location of the charged terminal groups is of primary concern. Our studies of polyelectrolytic dendrimers show that there is an ionic strength dependent, broad distribution of terminal groups instead of the delta function distribution considered in our earlier work. Thus, whereas von Goeler and Muthukumar considered a single charged shell, we model the dendrimer as a continuous series of concentric shells. Further, when we consider the shell lying at the radial distance Z away from the dendrimer's center, shells lying outside Z are assumed to be permeable to the polyelectrolyte chain. The impenetrable shell at Z accounts for the excluded-volume interaction. The charge−charge interaction between each shell and polymer segment is described by the spherically averaged Debye−Hückel interaction. This model is illustrated in Figure 12. Here, we have assumed that the terminal groups can fall between the radial distances A and B away from the center of dendrimer.

The total charge interaction between one polymer segment and the dendrimer is the sum of the segment's attractions to each shell. This potential is given by eq 7.

$$V = \frac{-4\pi l_B |q| e^{-\kappa r}}{\kappa r b} \frac{\Delta i}{\Delta a} \int_A^B da\ |\sigma(a)| a \sinh(\kappa a) \quad (7)$$

$\Delta i/\Delta a$ is the radial density of shells (1/length), l_B is the Bjerrum length, qe is the charge per segment, b is the bare polymer step length, r is the distance from the polymer segment to the center of the dendrimer, and $\sigma(a)$ (1/length^2) is the surface charge density due to the terminal groups on the shell situated at distance a away from the dendrimer's center.

Working within this picture and following the same essential steps as von Goeler and Muthukumar, we deduce the following as the criterion for complexation:

$$[1 - e^{-2\kappa Z}] \frac{l_B |q| \sigma_e}{b b_e \kappa^3} > \frac{0.12}{\pi} \quad (8)$$

b_e is the effective step length of the chain due to intramolecular interactions and is defined in terms of the radius of gyration, R_g, and chain length, L, by

$$R_g^2 = \frac{b_e L}{6} \quad (9)$$

The result is similar to the solution for the chain−sphere case except that the distribution of terminal groups contributes an effective sphere of radius Z and surface charge density, σ_e, defined as

$$\sigma_e = \frac{1}{\sinh(\kappa Z) Z} \frac{\Delta i}{\Delta a} \int_A^B da\ |\sigma(a)| a \sinh(\kappa a) \quad (10)$$

One requires values for A, B, $\sigma(a)$, $\Delta i/\Delta a$, and Z to utilize this prediction. Experimentally obtained knowledge of the terminal group distribution from scattering techniques will yield the former three. The latter two may be obtained via the conservation of charge constraint indicated by eq 11.

$$N_T = 4\pi Z^2 \frac{\sigma_e}{|q|} = \frac{4\pi}{|q|} \frac{\Delta i}{\Delta a} \int_A^B da\ |\sigma(a)| a^2 \quad (11)$$

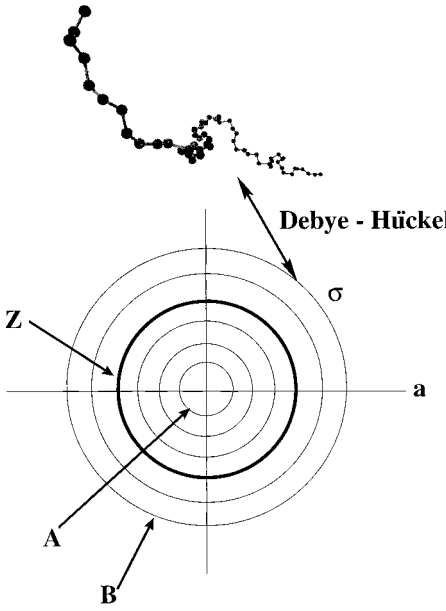

Figure 12. Charged concentric shell model for polymer−dendrimer complexation employed in theoretical analysis. Every shell except that falling at Z is permeable. All shells fall between A and B away from the center of the dendrimer. σ for each is determined by the dendritic terminal group distribution.

4.2. Comparison with Simulation. We compared our simulation results to our analytical prediction by first approximating $\sigma(a)$ based upon the isolated dendrimer's terminal group distribution using eq 12.

$$\langle \sigma(a) \rangle = \frac{\langle n(r) \rangle}{A_s(r)} \quad (12)$$

$\langle n(r) \rangle$ is the ensemble average number of beads between the shells at distances r and $r + dr$. $A_s(r)$ is the surface area of the shell falling at r. dr was set to $0.2 l_B$. We then fit a sixth-order polynomial to $\sigma(a)$. σ_e, Z, and $\Delta i/\Delta a$ were obtained via numerical integration using the mathematical software Mathematica version 3.0. A and B are also known from the isolated dendrimer simulations. The simulations of the isolated chains provided values for b_e via eq 9. b was taken to be l_o. The remaining

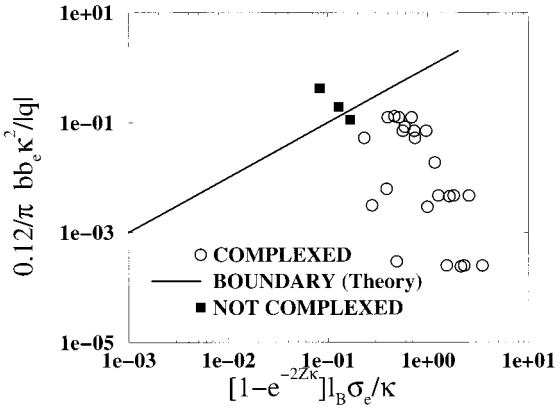

Figure 13. Simulation results for 60-bead chains complexing to fourth, fifth, and sixth generation dendrimers. $|q| = 1.0$, 0.5, and 0.1 κ^{-1} in the range $42.0l_B-0.8l_B$.

required values are simply input parameters from the simulation reflecting ionic strength and charge per bead. The prediction was found to be in excellent agreement with the simulations, as illustrated in Figure 13. Data for $N = 60$ chains, all generations of dendrimer, κ^{-1} in the range of $42.0l_B-0.80l_B$, and $|q| = 1.0-0.1$ are shown.

The vertical axis captures all the chain's variables while the horizontal axis represents those of the dendrimer. The line is the theoretical boundary for complexation. All points to the left of the line should not be complexed; all points to the right should be. A system was classified as noncomplexed if at any point in the simulation after the total interaction energy, $|E_a/k_BT|$, became nonzero, $|E_a/k_BT|$ fell below 10^{-6}. Typical values of $|E_a/k_BT|$ for systems with κ^{-1} just above the critical value were on the order of 10^{-2}. The difference in κ^{-1} between the two closest complexed and noncomplexed points in Figure 13 is only $1.0l_B$.

5. Discussion

These results address the nature of polyelectrolyte−dendrimer complexation and criteria for its occurrence, essential to our understanding and use of these materials as guest−host systems. The variational calculation suggests (i) that there is a critical effective dendritic charge density, (ii) that increasing the chain's stiffness reduces its interaction with the dendrimer, and (iii) that there is a critical ionic strength above which no complexation will occur. The former two predictions have been observed in the experimental studies found in the literature.[20−24] The latter is confirmed by our simulations. The simulations also indicate that complexes formed at lower salt concentrations may be disrupted by increasing the ionic strength to above the critical value. Difficulty in accomplishing this release experimentally has been noted by Kukowska-Latallo and coworkers.[20,21] However, strong noncharged secondary interactions such as hydrogen bonding may play an important role in maintaining the complex once formed and thus hinder a salt or pH triggered release.

The molecular weight and charge density not only play a decisive role in complex formation but also are important in determining the type of complex formed. If the chain is small and the dendrimer is large, the chain is encapsulated by the dendrimer. This encapsulation, in combination with the reversibility of complexation, is especially significant in the context of controlled delivery and also indicates that dendrimers should not be viewed as hard spheres. Conversely, if a smaller dendrimer and a larger chain are complexed, a significant chain density will lie outside of the dendrimer. The observation that the chain can penetrate a dendrimer is consistent with experimental studies.[24] Further, though highly soluble in a variety of solvents, dendrimers are occasionally observed to form aggregates.[38,39] The presence of chains loosely attached to the surface of the dendrimer may prove useful in such applications as steric stabilization of semidilute solutions of catalytic dendrimers. This stabilization is also suggested in the literature.[20,21] Finally, in the limit of large chains and small dendrimers, most closely reflecting a dendrimer−polymer system, novel "chain-walking" dynamics are observed. The mechanism of this behavior may be expected to play an important role in transporting polyelectrolytes and will be studied further in a later publication.

The simulations also indicate that the dimensions of both the dendrimer and chain change upon complexation. However, the extent to which the molecules shrink from their free solution sizes depends on how close the ionic strength is to its critical value. Further, in the limit of a large polyelectrolyte and small dendrimer, the chain collapses only in the vicinity of the dendrimer, yielding a smaller change in dimension.

6. Conclusions

We have examined the dilute solution nature of complexes of dendrimers with charged terminal groups and oppositely charged polyelectrolytes via Monte Carlo simulation and variational theory. Critical values of salt concentration, dendrimer charge density, and chain stiffness were noted. Three types of reversible complexes were observed. Under the proper conditions, a dendrimer may encapsulate a chain, a chain may interpenetrate a dendrimer, or a unique "chain-walking" phenomenon may be observed. Though both chain and dendrimer undergo a shrinkage in size upon complexation, the extent of the rearrangement depends on the proximity of the system to the complexation threshold and the relative shielding ability of the two molecules.

Acknowledgment is made to NSF Grant DMR 9970718. The authors are also grateful to Joey Kong and Gustavo Carri for many fruitful conversations and guidance regarding the problem addressed here.

Appendix

Here we provide a brief derivation of our prediction for the critical complexation conditions given by eq 8 in the text. The polyelectrolyte chain in the presence of our concentric shell model dendrimer is characterized by the end-to-end vector probability, $G[\vec{R}_e;0,L]$. $\vec{R}_e \equiv \vec{R}_0 - \vec{R}_L$ is the end-to-end vector, and L is the chain contour length. The Edwards' path integral[3,40] description for $G[\vec{R}_0,\vec{R}_L;0,L]$ is

$$G[\vec{R}_e;0,L] = \int_{\vec{R}(0)=\vec{R}_0}^{\vec{R}(L)=\vec{R}_L} D[\vec{R}(s)] \times \exp\left[-\frac{3}{2b}\int_0^L ds\left(\frac{\delta\vec{R}(s)}{\delta s}\right)^2 - \int_0^L ds\,\Upsilon[\vec{R}(s)]\right] \quad \text{(A1)}$$

s is the chain contour position variable, and $\vec{R}(s)$ is the location of the chain segment that lies at s along the backbone. $\int_{\vec{R}(0)=\vec{R}_0}^{\vec{R}(L)=\vec{R}_L} D[\vec{R}(s)]$ denotes integration over all possible configurations for $\vec{R}(s)$. The first integral in the exponential captures the chain's connectivity. The sec-

ond represents the chain segments' nonbonded interactions with itself and the model dendrimer. Explicitly,

$$\int_0^L \mathrm{d}s \Upsilon[\vec{R}(s)] = \frac{w}{2b^2}\int_0^L \mathrm{d}s \int_0^L \mathrm{d}s'\, \delta[\vec{R}(s) - \vec{R}(s')] + \frac{l_B|q^2|}{2b^2}\int_0^L \mathrm{d}s \int_0^L \mathrm{d}s' \frac{e^{[-\kappa|\vec{R}(s)-\vec{R}(s')|]}}{|\vec{R}(s) - \vec{R}(s')|} - \frac{4\pi l_B|q|}{b}\frac{\Delta i}{\Delta a}\int_0^L \mathrm{d}s \frac{e^{[-\kappa|\vec{R}(s)|]}}{\kappa|\vec{R}(s)|}\int_A^B \mathrm{d}a\, |\sigma(a)| a \sinh(\kappa a) \quad \text{(A2)}$$

The first term represents the chain's excluded-volume intramolecular interactions. The excluded-volume parameter is given by the binary cluster integral:

$$w = \int \mathrm{d}\vec{r}\, [1 - e^{-u_E/k_B T}] \quad \text{(A3)}$$

$u_E/k_B T$ is given by the second term of eq 5 in the text. The chain's intramolecular charge−charge repulsion is approximated by the Debye−Hückel potential in the second term. The third term is the attractive interaction between the concentric shells and the chain. Note that we have placed the origin at the center of the model dendrimer.

We are interested primarily in how the interaction between the chain and the model dendrimer affects the complexation requirements and are not interested in the chain's internal degrees of freedom. Therefore, we assume that the first two terms in eq A2, the chain's self-interactions, have the effect of creating an effective step length, b_e, as defined by eq 9 in the text. Thus, the analysis is simplified to investigating a random walk of chain segments that interact with the model dendrimer via the potential in eq 7. With this approximation, the end-to-end vector probability is given by

$$G[\vec{R}_e;0,L] = \int_{\vec{R}(0)=\vec{R}_0}^{\vec{R}(L)=\vec{R}_L} D[\vec{R}(s)] \times \exp\left[-3/(2b_e)\int_0^L \mathrm{d}s \left(\frac{\delta\vec{R}(s)}{\delta s}\right)^2 + \frac{4\pi l_B|q|}{b}\frac{\Delta i}{\Delta a}\int_0^L \mathrm{d}s \frac{\exp[-\kappa|\vec{R}(s)|]}{\kappa|\vec{R}(s)|} \times \int_A^B \mathrm{d}a \left|\sigma(a)\right| a \sinh(\kappa a)\right] \quad \text{(A4)}$$

Equivalently, $G[\vec{R}_e;0,L]$ must satisfy

$$\left[\frac{\delta}{\delta L} - \frac{b_e}{6}\vec{\nabla}_{\vec{R}_e}{}^2 + V\right] G[\vec{R}_e;0,L] = \delta(\vec{R}_e)\,\delta(L) \quad \text{(A5)}$$

with the implicit boundary conditions that $G[\vec{R}_e;0,L] = 0$ at the surface of our impenetrable shell at Z and $\lim_{\vec{R}_e \to \infty} G[\vec{R}_e;0,L] = 0$. V is given by eq 7 in the text.

This differential form may be further simplified into a spherically symmetric eigenvalue problem. We begin to do this by introducing the bilinear expansion of $G[\vec{R}_e;0,L]$,

$$G[\vec{R}_e;0,L] = \sum_{\alpha=1}^{\infty} \Psi_\alpha^*(\vec{R}_L)\, \Psi_\alpha(\vec{R}_0) e^{-\lambda_\alpha L} \quad \text{(A6)}$$

where $\Psi_\alpha(\vec{R})$ is the αth eigenfunction and λ_α is the corresponding eigenvalue of the operator

$$\hat{H} = \frac{-b_e}{6}\vec{\nabla}_{\vec{R}}{}^2 + V \quad \text{(A7)}$$

Since we are interested in the high molecular weight limit, $L \gg 1$, the ground-state Ψ_0 will dominate[40,41] the sum in eq A6. Thus, we have

$$G[\vec{R}_e;0,L] \approx \Psi_0^*(\vec{R}_L)\, \Psi_0(\vec{R}_0) e^{-\lambda_0 L} \quad \text{(A8)}$$

with $\Psi_0(\vec{R})$ satisfying

$$\left[\frac{-b_e}{6}\vec{\nabla}_{\vec{R}}{}^2 + V\right]\Psi_0(\vec{R}) = \lambda_0 \Psi_0(\vec{R}) \quad \text{(A9)}$$

We now take advantage of the spherical symmetry of the problem and obtain

$$\hat{H}'\Psi_0 = \lambda'\Psi_0 \quad \text{(A10)}$$

where we have defined

$$\hat{H}' \equiv -\frac{1}{\Gamma^2}\frac{\delta}{\delta\Gamma}\left(\Gamma^2 \frac{\delta()}{\delta\Gamma}\right) + \frac{E e^{-\Gamma}}{\Gamma} \quad \text{(A11)}$$

$$E \equiv \frac{-24\pi l_B|q|}{\kappa^2 b_e b}\frac{\Delta i}{\Delta a}\int_A^B \mathrm{d}a\, |\sigma(a)| a \sinh(\kappa a) \quad \text{(A12)}$$

$\Gamma \equiv \kappa r$, and $\lambda' \equiv 6\lambda_0/(b_e\kappa^2)$. Unfortunately, there is no known exact analytical solution to this equation for Ψ_0. We therefore proceed with the variational approach. The technique is to guess a functional form for Ψ_0 based upon the boundary conditions stated above for $G[\vec{R}_e;0,L]$. We choose

$$\Psi_0 = \frac{\Gamma - \Gamma_0}{\Gamma} e^{-\nu\Gamma} \quad \text{(A13)}$$

Here, we have defined $\Gamma_0 \equiv \kappa Z$ with Z being our hard-core radius. The test function is expressed in terms of a variational parameter, ν, that may be adjusted to minimize the energy of the system. Within this approach, λ' is estimated using eq A14.

$$\lambda' = \frac{\int_{\Gamma_0}^{\infty} \mathrm{d}\Gamma\, \Gamma^2 \hat{H}'\Psi_0}{\int_{\Gamma_0}^{\infty} \mathrm{d}\Gamma\, \Gamma^2 \Psi_0} = \frac{\nu^3}{\nu\Gamma_0 + 2}\left[\Gamma_0 + e^{-\Gamma_0}\frac{E}{(\nu+1)^2}\right] \quad \text{(A14)}$$

Complexed states are those that correspond to $\lambda' < 0$ with $\nu > 0$. The first term in the product is positive for $\nu > 0$, and the term within the bracket is monotonically increasing for $\nu > 0$. Thus, the necessary and sufficient condition for a bound state to exist is

$$(1 - e^{-2\kappa Z})\frac{12\pi|q|l_B\sigma_e}{\kappa^3 b_e b} > 1 \quad \text{(A15)}$$

Finally, we account for lost normalization prefactors by correcting our prediction with the known solution for planar adsorption[3] and obtain eq 8 in the text.

References and Notes

(1) Weigel, F. W. *J. Phys. A* **1977**, *10*, 299.
(2) Hesselink, F. T. J. *J. Colloid Interface Sci.* **1977**, *60*, 448.
(3) Muthukumar, M. *J. Chem. Phys.* **1987**, *86*, 7230.
(4) Varoqui, R. In *Macro-ion Characterization: From Dilute Solutions to Complex Fluids*; Schmitz, K. S., Ed.; American Chemical Society: Washington, DC, 1994.
(5) von Goeler, F.; Muthukumar, M. *J. Chem. Phys.* **1994**, *100*, 7796.
(6) Muthukumar, M. *J. Chem. Phys.* **1995**, *103*, 4723.
(7) Châtellier, X.; Joanny, J. F. *J. Phys. II* **1996**, *6*, 1669.

(8) Muthukumar, M. In *Interfacial Aspects of Multicomponent Polymer Materials*; Lohse, D. J., Russell, T. P., Sperling, L. H., Eds.; Plenum Press: New York, 1997.
(9) Haronska, P.; Vilgis, T. A.; Grottenmüller, R.; Schmidt, M. *Macromol. Theory Simul.* **1998**, *7*, 241.
(10) Muthukumar, M. *Curr. Opin. Colloid Interface Sci.* **1998**, *3*, 48.
(11) Bruinsma, R.; Mashl, J. *Europhys. Lett.* **1998**, *41*, 165.
(12) Rudnick, J.; Bruinsma, R. *Biophys. J.* **1999**, *76*, 1725.
(13) Srivastava, D.; Muthukumar, M. *Macromolecules* **1994**, *27*, 1461.
(14) Wallin, T.; Linse, P. *Langmuir* **1996**, *12*, 305; *J. Phys. Chem.* **1996**, *100*, 17873; *J. Phys. Chem. B* **1997**, *101*, 5506.
(15) Kong, C. Y.; Muthukumar, M. *J. Chem. Phys.* **1998**, *109*, 1522.
(16) Matthews, O. A.; Shipway, A. N.; Stoddart, J. F. *Prog. Polym. Sci.* **1998**, *23*, 1 and references therein.
(17) Jansen, J. F. G. A.; de Brabander-van den Berg, E. M. M.; Meijer, E. W. *Science* **1994**, *266*, 1226.
(18) Jansen, J. F. G. A.; Meijer, E. W.; de Brabander-van den Berg, E. M. M. *Macromol. Symp.* **1996**, *102*, 27.
(19) Margerum, L. D.; Campion, B. K.; Koo, M.; Shargill, N.; Lai, J. J.; Marumoto, A.; Sontum, P. C. *J. Alloys Compd.* **1997**, *249*, 185.
(20) Kukowska-Latallo, J. F.; Bielinska, A. U.; Johnson, J.; Spindler, R.; Tomalia, D. A.; Baker, J. R. *Proc. Natl. Acad. Sci. U.S.A.* **1996**, *93*, 4897.
(21) Bielinska, A.; Kukowska-Latallo, J. F.; Johnson, J.; Tomalia, D. A.; Baker, J. R. *Nucl. Acids Res.* **1996**, *24*, 2176.
(22) Ottaviani, M. F.; Sacchi, B.; Turro, N. J.; Chen, W.; Jockusch, S.; Tomalia, D. A. *Macromolecules* **1999**, *32*, 2275.
(23) Li, Y.; Dubin, P. L.; Spindler, R.; Tomalia, D. A. *Macromolecules* **1995**, *28*, 8426.
(24) Kabanov, V. A.; Zezin, A. B.; Rogacheva, V. B.; Gulyaeva, Zh. G.; Zansochva, M. F.; Joosten, J. G. H.; Brackman, J. *Macromolecules* **1999**, *32*, 1904.
(25) Tomalia, D. A.; Baker, H.; Dewald, J.; Hall, M.; Kallos, G.; Martin, S.; Roeck, J.; Ryder, J.; Smith, P. *Polym. J.* **1985**, *17*, 117.
(26) de Brabander-van den Berg, E. M. M.; Meijer, E. W. *Angew. Chem., Int. Ed. Engl.* **1993**, *32*, 1308.
(27) Armstrong, R. *J. Chem. Phys.* **1974**, *60*, 724.
(28) McQuarrie, D. *Statistical Mechanics*; Harper Collins: New York, 1976.
(29) Milchev, A.; Binder, K. *Macromol. Theory Simul.* **1994**, *3*, 915.
(30) Welch; P. M.; Mathias, L. J.; Lescanec, R. L. *Polym. Prepr.* **1996**, *37*, 250.
(31) Welch, P.; Muthukumar, M. *Macromolecules* **1998**, *31*, 5892.
(32) Metropolis, N.; Rosenbluth, A. W.; Rosenbluth, M. N.; Teller, A. H.; Teller, E. J. *J. Chem. Phys.* **1953**, *21*, 1098.
(33) Binder, K.; Heermann, D. W. *Monte Carlo Simulation in Statistical Physics*; Springer-Verlag: New York, 1992.
(34) Lescanec, R. L.; Muthukumar, M. *Macromolecules* **1990**, *23*, 2280.
(35) de Gennes, P.-G.; Hervet, H. *J. Phys., Lett.* **1983**, *44*, L351.
(36) Murat, M.; Grest, G. *Macromolecules* **1996**, *29*, 178.
(37) Mansfield, M.; Klushin, L. *Macromolecules* **1993**, *26*, 4262.
(38) Briber, R.; Bauer, B.; Hammouda, B.; Tomalia, D. *Polym. Mater. Sci. Eng.* **1992**, *67*, 430.
(39) Scherrenberg, R.; Coussens, B.; van Vliet, P.; Edouard, G.; Brackman, J.; de Brabander, E. *Macromolecules* **1998**, *31*, 456.
(40) Edwards, S. F. *Proc. Phys. Soc.* **1965**, *85*, 613.
(41) de Gennes, P.-G. *Rep. Prog. Phys.* **1969**, *32*, 187.

MA000021D